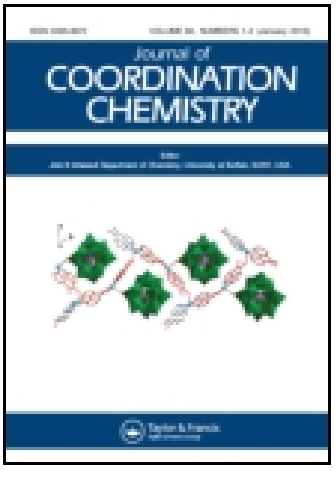

Journal of Coordination Chemistry
Publication details, including instructions for authors and subscription information:
http://www.tandfonline.com/loi/gcoo20

Synthesis, characterization, and pharmacological aspects of metal(II) complexes incorporating 4-[phenyl(phenylimino)methyl]benzene-1,3-diol

P. Subbaraj[a], A. Ramu[b], N. Raman[c] & J. Dharmaraja[d]

[a] Department of Chemistry, Devanga Arts College, Aruppukottai, India

[b] Department of Inorganic Chemistry, School of Chemistry, Madurai Kamaraj University, Madurai, India

[c] Research Department of Chemistry, V.H.N.S.N. College, Virudhunagar, India

[d] Department of Science and Humanities, Sree Sowdambika College of Engineering, Aruppukottai, India

Accepted author version posted online: 30 Jul 2014.Published online: 22 Aug 2014.

To cite this article: P. Subbaraj, A. Ramu, N. Raman & J. Dharmaraja (2014) Synthesis, characterization, and pharmacological aspects of metal(II) complexes incorporating 4-[phenyl(phenylimino)methyl]benzene-1,3-diol, Journal of Coordination Chemistry, 67:16, 2747-2764, DOI: 10.1080/00958972.2014.950256

To link to this article: http://dx.doi.org/10.1080/00958972.2014.950256

Journal of Coordination Chemistry, 2014
Vol. 67, No. 16, 2747–2764, http://dx.doi.org/10.1080/00958972.2014.950256

Synthesis, characterization, and pharmacological aspects of metal(II) complexes incorporating *4-[phenyl(phenylimino) methyl]benzene-1,3-diol*

P. SUBBARAJ†, A. RAMU‡, N. RAMAN*§ and J. DHARMARAJA¶

†Department of Chemistry, Devanga Arts College, Aruppukottai, India
‡Department of Inorganic Chemistry, School of Chemistry, Madurai Kamaraj University, Madurai, India
§Research Department of Chemistry, V.H.N.S.N. College, Virudhunagar, India
¶Department of Science and Humanities, Sree Sowdambika College of Engineering, Aruppukottai, India

(*Received 10 February 2014; accepted 26 June 2014*)

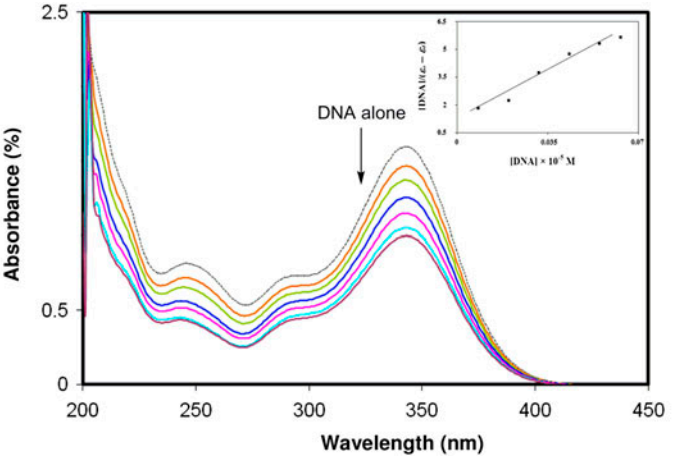

The *4-[phenyl(phenylimino)methyl]benzene-1,3-diol* Schiff base metallointercalators act as efficient DNA binding and cleaving agents. All the complexes are *in vitro* biological and antioxidant activators. Cu(II) complex is found to be efficient intercalator than other chelates.

New metallointercalators (**1a**–**1e**) have been synthesized using the Schiff base, *4-[phenyl(phenylimino) methyl]benzene-1,3-diol* and metal(II) ions, *viz*. Mn(II), Co(II), Ni(II), Cu(II), and Zn(II). They are characterized by analytical and spectral methods. Elemental analyses and molar conductance values reveal that the Schiff base metal(II) complexes have 1 : 2 stoichiometry and are non-electrolytes. The Schiff base (HL) binds with M(II) ions through azomethine and deprotonated phenolic groups. Thermal studies reveal the presence of water in **1a**–**1c**. Powder X-ray diffraction and SEM studies show that all the complexes are microcrystalline with homogenous morphology. *In vitro* biological activities of HL and **1a**–**1e** have been screened against bacteria and fungi by well diffusion

*Corresponding author. Email: support@vhnsnc.edu.in

technique, revealing that these complexes are good antimicrobial agents against various pathogens. The complexes exhibit better biological activities than HL. Complex **1d** binds with Calf thymus DNA through intercalation and weak covalent interactions. The oxidative cleavage of **1a**–**1e** with *pUC* 19 DNA has also been explored. The results indicate that they bind to DNA through intercalation and are efficient metallointercalators and cleaving agents.

Keywords: Benzophenone; Schiff base metal(II) complexes; Metallointercalators; Biological activity; DNA cleavage

1. Introduction

Mutation of genes and therapeutic approaches in transition metal complexes has been paid much attention [1, 2]. Schiff bases having sp^2-hybridized nitrogen of the azomethine (–HC=N–) play a central role in transition metal complexes. Schiff base complexes have been studied for their various structures, steric effects, and coordination chemistry [3, 4]. Transition metal complexes of benzophenones exhibit biological activity including antibacterial [5], antifungal [6], antitumor [7], and herbicidal [8] activities. Benzophenone derivatives also exhibit activities in primary anti-HIV screening [9]. Transition metal complexes of aniline and its substituted moieties, pharmacological activities, spectral studies, DNA binding [10–13], and cleavage of such ligands and their complexes [14–16] have also been reported. In the chemistry of nucleic acids, transition metal complexes play a vital role to bind and cleave DNA under certain physiological conditions [17, 18]. Interaction of DNA with metal complexes [19] has been paid much attention. In this paper, we report the synthesis and characterization of ML_2 complexes (where M = Mn(II), Co(II), Ni(II), Cu(II), and Zn(II); L = 4-[phenyl(phenylimino)methyl]benzene-1,3-diol of NO type). We have investigated the DNA-binding behavior of Schiff base metal(II) complexes by various spectral techniques. We have measured the antimicrobial activity of the HL and its metal complexes (**1a**–**1e**) against various bacterial strains (*Escherichia coli*, *Staphylococcus saphyphiticus*, *Staphylococcus aureus*, and *Pseudomonas aeruginosa*) and fungal strains (*Aspergillus niger*, *Enterobacter species*, and *Candida albicans*) by well diffusion technique.

2. Experimental

2.1. *Materials and reagents*

All reagents and chemicals were purchased from extra pure Sigma Products and used as such. Solvents were purified by standard procedures [20]. Calf thymus (CT) DNA was purchased from Bangalore Genei (India). Agrose (Molecular Biology Grade) and ethidium bromide (EB) were obtained from Sigma (USA). Tris–HCl [(hydroxymethyl)aminomethane–HCl] buffer solution was prepared using deionized and sonicated triple-distilled water using a quartz water distillation setup.

2.2. *Instruments*

Melting points of the complexes were determined in open glass capillaries and are uncorrected. Elemental analyses of HL and its metal complexes were carried out on a CHN analyzer Carlo Erba 1108, Heraeus. Conductance measurements were made using 10^{-3} M solutions of complexes in DMF using an Elico conductivity bridge (Model No. CM 180). IR spectra were recorded from 400 to 4000 cm^{-1} using a Perkin Elmer 783 series FTIR spectrophotometer. Magnetic susceptibility measurements on powder samples were carried out by Gouy's method using $Hg[Co(SCN)_4]$ as calibrant and diamagnetic corrections were applied in compliance with Pascal's constant [21]. From a Shimadzu UV-1601 spectrophotometer, the electronic spectra from 200 to 1100 nm were obtained. ^1H NMR spectra of HL and its zinc complex (**1e**) in DMSO-d_6 were recorded on a Bruker Avance DRX 300 FT NMR spectrometer using TMS as internal standard. Fast atomic bombardment-mass spectra (FAB-MS) were recorded using a VGZAB-HS spectrometer in a 3-nitrobenzylalcohol matrix. X-band EPR spectrum of Cu(II) complex in DMSO at room temperature (300 K) and liquid nitrogen conditions (77 K) were recorded on a VARIAN E-112 spectrometer using DPPH as internal standard. Thermograms were recorded in a dynamic N_2 atmosphere (flow rate 20 mL min^{-1}) with a heating rate of 10 K min^{-1} using a Perkin Elmer (TGS-2 model) thermal analyzer. Powder X-ray diffraction (XRD) patterns were recorded with a Bruker AXS D8 Advance powder X-ray diffractometer (X-ray source: Cu, wavelength 1.5406 Å). Si(Li)PSD was used as a detector. Scanning electron micrography with energy-dispersive spectrometry associated (SEM/EDS) was used for morphological evaluation. DNA binding was recorded in DMF solution with a Shimadzu UV-1601 spectrophotometer, and oxidative DNA cleavage activities were monitored by agarose gel electrophoresis instrument.

2.3. *Synthesis of Schiff base metal(II) complexes*

HL was synthesized as previously reported [12]. Schiff base complexes **1a**–**1e** were synthesized by mixing HL (10 mM, in 10 mL of absolute ethanol) to the dropwise added corresponding metal salts: $Mn(CH_3COO)_2{\cdot}4H_2O$, $Co(CH_3COO)_2{\cdot}4H_2O$, $Ni(CH_3COO)_2{\cdot}4H_2O$, $Cu(CH_3COO)_2{\cdot}H_2O$, and $Zn(CH_3COO)_2{\cdot}2H_2O$ (5 mM in 10 mL of ethanol) having the required molar ratio of 1 : 2 (metal : ligand). After addition, the reaction mixture was refluxed for a time depending on the metal salt used [6 h for Mn(II), 5.30 h for Co(II), 5 h for Ni(II), 4 h for Cu(II), and 4.30 h for Zn(II)] and the resulting solution was reduced to half of its original volume using a water bath and kept at room temperature. On standing, the obtained solid products were filtered by *vacuum* filtration, washed several times with water, ethanol, diethyl ether, and finally dried *in vacuo* over anhydrous $CaCl_2$ (figure 1).

2.4. In vitro *biological studies*

In vitro biological activity of **1a**–**1e** was tested against four pathogenic bacteria (*E. coli*, *S. saphyphiticus*, *S. aureus*, and *P. aeruginosa*) using Muller Hinton agar nutrient and three fungi (*A. niger*, *E. species*, and *C. albicans*) using potato dextrose agar as the medium by the well diffusion technique [14, 22].

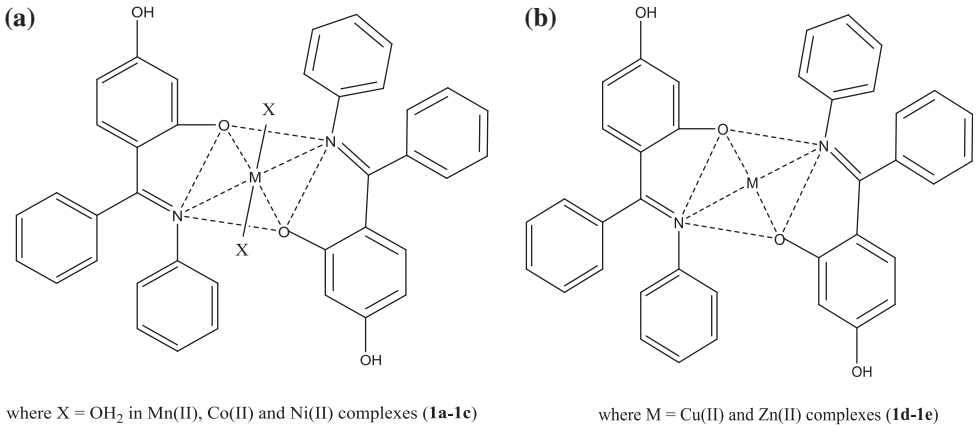

where X = OH_2 in Mn(II), Co(II) and Ni(II) complexes (**1a-1c**)

where M = Cu(II) and Zn(II) complexes (**1d-1e**)

Figure 1. Proposed structure for Schiff base metal(II) complexes.

2.5. *Antioxidant activity*

The *in vitro* antioxidant activities of HL and its metal(II) complexes have been investigated at room temperature by the Blois method [23]. One milliliter of different concentration (10, 20, 30, 40, and 50 μM) solutions of HL and its metal(II) complexes was taken in different test tubes and 4 mL of a 0.1 mM ethanolic DPPH solution was added to each and the reaction mixture was shaken vigorously *ca.* 2–3 min. The reaction mixture was kept *ca.* 20–30 min at room temperature. A blank DPPH solution prepared without compound was used for the baseline correction. After incubation, the absorbance values (λ_{max}) for each compound were measured at 517 nm using a UV–visible spectrophotometer. There was a change (decrease) in the absorbance values (λ_{max}) which indicated that the complexes show moderate free radical scavenging activities. Ascorbic acid was used as the reference or positive control. Free radical scavenging effects in percentage was calculated using this formula as:

$$\text{Scavenging effects}\,(\%) = \left[\frac{(A_{\text{control}} - A_{\text{sample}})}{A_{\text{control}}}\right] \times 100$$

where A_{control} = absorbance of the control (blank, without the ligand or complex) and A_{sample} = absorbance of the ligand or complex. All the analyses were made in triplicate for each and the results were compared with the control.

2.6. *Interaction between metal(II) complexes with DNA*

DNA-binding experiments were done in Tris–HCl/NaCl buffer (5 mM Tris–HCl, 50 mM NaCl, pH 7.2) with metal complexes in DMF solution [24–26]. CT DNA concentration was determined by UV absorbance at 260 nm using $\varepsilon = 6600\ M^{-1}\ cm^{-1}$. The purity of the CT DNA was checked by its absorbance values at 260 nm, 280 nm, and the ratio A_{260}/A_{280} was 1.87, indicating that CT DNA was sufficiently free from protein contamination [27]. Stock solutions were kept at 4 °C and used after not more than four days. Doubly distilled H_2O was used to prepare the buffer.

2.6.1. Absorption studies. Electronic spectra of the metal complexes (10^{-5} M) were recorded before and after addition of CT DNA. Experiments were done by keeping the metal complex concentration as constant while varying the concentration of CT DNA (r = 0.0, 0.20, 0.40, 0.60, 0.80, and 1.00; where r is the molar ratio of DNA and complex). After the addition of CT DNA, the resulting mixture was shaken and allowed to equilibrate for 5–10 min at room temperature. Absorption readings (corresponding to the changes at maximum absorption) were recorded after each successive addition of CT DNA solution. To know quantitatively the binding strength of the metal complexes with increasing concentration of DNA using equation [28],

$$\frac{[\mathrm{DNA}]}{(\varepsilon_a - \varepsilon_f)} = \frac{[\mathrm{DNA}]}{(\varepsilon_b - \varepsilon_f)} + \frac{1}{K_b(\varepsilon_b - \varepsilon_f)}$$

where ε_f, ε_b, and ε_a are the molar extinction coefficients of the free complex in solution, the complex is in completely bound form with CT-DNA and is complex bound to DNA at a definite concentration, respectively. In the plot of [DNA]/($\varepsilon_a - \varepsilon_f$) *versus* [DNA], K_b was calculated.

2.6.2. Fluorescence studies. The fluorescence spectra were recorded at room temperature with excitation at 520 nm and emission at 1600 nm. Fluorescence spectra of the complexes were recorded before and after the addition of DNA in the presence of 5 mM Tris–HCl/50 mM NaCl buffer. A fixed concentration value of the complex (10^{-3} M) was titrated with increasing amounts of DNA [29] from 20 to 100 μM and 1.0×10^{-5} M EB.

2.6.3. DNA cleavage activities. DNA cleavages of HL and **1a**–**1e** were monitored by agarose gel electrophoresis on CT DNA. Gel electrophoresis experiments were performed under aerobic condition with an oxidant (H_2O_2) by incubation at 35 °C for 2 h as follows: CT DNA 30 μM, 50 μM of each complex, 50 μM of oxidant in 50 mM Tris–HCl buffer (pH 7.2) containing 50 mM NaCl solution. After incubation, 1 μL of loading buffer (bromophenol blue in water) was added to each tube and the samples were loaded on 1% agarose gel. Samples were electrophoresed at a constant voltage (50 V) for 2 h in Tris–acetic acid–EDTA buffer (pH 8.3). After electrophoresis, the gel was stained for 30 min by immersing it in 1 μg/cm^3 EB solution. DNA cleavage was visualized by viewing the gel under ultraviolet (UV) light and photographed.

3. Results and discussion

Schiff base metal(II) complexes (**1a**–**1e**) were synthesized and characterized by various spectroscopic techniques. They are quite air stable at room temperature, non-hygroscopic, and insoluble in water but readily soluble in DMF and DMSO. Analytical data, molar conductivities, and magnetic moment data are presented in table 1. Analytical data show that all the complexes have 1 : 2 stoichiometric ratio (metal : ligand). Molar conductance values indicate that they are non-electrolytes [30].

Table 1. Elemental and physical data of HL and its metal(II) complexes.

Compound	Empirical formula	Formula weight	Color	M.p. (°C)	Yield (%)	Elemental analysis found (Calcd) % M	C	H	N	Λ_M ($\Omega^{-1}M^{-1}cm^2$)
1a	$C_{38}H_{32}MnN_2O_6$	667	Reddish brown	272	69	7.99 (8.12)	68.72 (68.86)	4.91 (4.84)	4.24 (4.02)	14.5
1b	$C_{38}H_{32}CoN_2O_6$	635	Pink	268	72	8.29 (8.40)	68.55 (67.84)	4.82 (4.76)	3.90 (4.10)	16.9
1c	$C_{38}H_{32}NiN_2O_6$	670	Pale green	260	70	8.42 (8.77)	68.41 (67.49)	4.74 (4.46)	4.12 (4.29)	17.2
1d	$C_{38}H_{28}CuN_2O_4$	640	Brown	276	65	10.01 (9.93)	70.97 (71.29)	4.34 (4.41)	4.45 (4.38)	14.6
1e	$C_{38}H_{28}ZnN_2O_4$	641	Pale yellow	>280	62	10.06 (10.19)	70.89 (71.09)	4.29 (4.40)	4.45 (4.36)	15.8

3.1. *IR spectra*

Comparison of IR spectra of HL and **1a**–**1e** will be useful to determine the chelation. Major change in $\nu_{C=N}$ (azomethine) of HL shifted from 1598 to 1580–1572 cm^{-1} in spectra of metal complexes. Additionally, ν_{OH} (phenolic–OH) is also shifted from 1245 to 1261–1277 cm^{-1} in the complexes. These observations indicate that azomethine nitrogen and deprotonated phenolic OH are involved in chelation [31, 32]. Weak-to-medium intensity bands are observed in the metal complexes at 400–500 and 560–580 cm^{-1} which correspond to ν(M–O) and ν(M–N), and these peaks are absent in the free ligand [31, 32]. The presence of coordinated water in metal complexes (except **1d** and **1e**) is indicated by a broad band at 3300–3450 cm^{-1} and two weaker bands at 814–857 and 705–720 cm^{-1} due to –OH rocking and wagging vibrations, respectively [31–33].

3.2. *Electronic spectral and magnetic moment studies*

Electronic spectra of HL and its metal(II) complexes were measured at room temperature in DMF solution from 200 to 1100 nm. Various spectral data (B, B', β, β (%) and LFSE) for Co(II) and Ni(II) complexes (table 2) were calculated by applying band energies on Tanabe Sugano diagrams. Complex **1a** shows sharp and weak absorptions at 16,447 cm^{-1} probably due to $^4A_{1g} \rightarrow {}^4T_{1g}$ (^4G) transition [35]. In d^5, electronic configuration of high-spin Mn(II) complexes show an effective magnetic moment value, 6.0 BM, which is very close to our value, 5.78 BM, confirming octahedral environment around Mn(II) with five unpaired electrons [34, 35]. Complex **1b** exhibits three spin-allowed transitions at 9750, 13,300, and 19,630 cm^{-1} assigned to $^4T_{1g}$ (F) $\rightarrow {}^4T_{2g}$ (F), $^4T_{1g}$ (F) $\rightarrow {}^4A_{2g}$ (F), and $^4T_{1g}$ (F) $\rightarrow {}^4T_{1g}$ (P), respectively, suggesting a distorted

Table 2. Electronic absorption spectral data (in DMF) and magnetic susceptibility of **1a**–**1e**.

					Ligand field parameter					
Complex	λ_{max} (cm^{-1})	Band assignments	Geometry	μ_{eff} (BM)	Dq (cm^{-1})	B (cm^{-1})	β	β (%)	LFSE (kJ M^{-1})	ν_2/ν_1
1a	16,447	$^6A_{1g} \rightarrow {}^4T_{1g}$ (^4G)	Distorted octahedral	5.78	–	–	–	–	–	–
1b	9750	$^4T_{1g}$ (F) $\rightarrow {}^4T_{2g}$ (F)	Distorted octahedral	4.88	1091	735.87	0.76	24	104.32	1.36
	13,300	$^4T_{1g}$ (F) $\rightarrow {}^4A_{2g}$ (F)				(971 for free ion)				
	19,630	$^4T_{1g}$ (F) $\rightarrow {}^4T_{1g}$ (P)								
1c	10,256	$^3A_{2g}$ (F) $\rightarrow {}^3T_{2g}$ (F)	Distorted octahedral	3.15	1026	650.27	0.63	36.89	357.01	1.55
	15,949	$^3A_{2g}$ (F) $\rightarrow {}^3T_{1g}$ (F)				(1030 for free ion)				
	24,570	$^3A_{2g}$ (F) $\rightarrow {}^3T_{1g}$ (P)								
	29,851	LMCT ($n \rightarrow \pi^*$)								
1d	11,442	d–d envelope	Distorted tetrahedral	1.96	–	–	–	–	–	–
	26,280	LMCT ($n \rightarrow \pi^*$)								
1e	26,385 (b)	LMCT (M $\leftarrow$ N)	Tetrahedral	Dia.	–	–	–	–	–	–

octahedral geometry [34, 35]. The ratio of v_2/v_1 is 1.36 as expected for octahedral geometry and the magnetic moment value (4.88 BM) of the complex indicating four unpaired electrons with the high-spin six-coordinate octahedral environment around cobalt(II) [34]. Complex **1c** shows four bands at 10,256, 15,949, 24,570, and 29,851 cm^{-1} which are assigned to $^3A_{2g}$ (F) $\rightarrow$ $^3T_{2g}$ (F), $^3A_{2g}$ (F) $\rightarrow$ $^3T_{1g}$ (F), $^3A_{2g}$ (F) $\rightarrow$ $^3T_{1g}$ (P), and L $\rightarrow$ M charge transfer, respectively, with a distorted octahedral geometry with $^3A_{2g}$ as ground state [34, 36]. Absence of any band below 10,000 cm^{-1} rules out a tetrahedral environment. Observed magnetic moment value (3.15 BM) corresponds to two unpaired electrons per Ni(II) ion for the six-coordinate octahedral environment with $D_{4\ h}$ symmetry [36, 37]. Complex **1d** exhibits one LMCT band at 26,280 cm^{-1} and another unsymmetrical broad absorption centered at 11,442 cm^{-1} that can be assigned to d–d electronic transition [35]. This low-energy absorption band with less intensity is commonly found in distorted tetrahedral Cu(II) complex and is produced by Jahn–Teller distortion. The observed magnetic moment (1.96 BM) is within the predictable region (1.92–2.00 BM) found for distorted tetrahedral environment [35]. Zinc (II), which is diamagnetic, does not show any d–d transition in the visible region. However, **1e** shows only one broad band centered at 26,385 cm^{-1} in the UV region due to L $\rightarrow$ M charge transfer in tetrahedral environment [35]. Ligand field parameters such as Racah parameter (B), β, and β° values support the covalent character of the distorted octahedral geometry around Ni(II) and Co(II) complexes [36]. Mixing of ground state ($^3A_{2g}$) with the excited state ($^3T_{2g}$) in octahedral Ni(II) complex gives the Lunde's factor, i.e. $g = 2 - \frac{8\lambda'}{10Dq}$ (where λ' = spin–orbit coupling constant, $-368\ cm^{-1}$). In general, the hexaaquo Ni(II) complex shows the g value 2.25; for our complex (**1c**) the g value is 2.287 [36, 37].

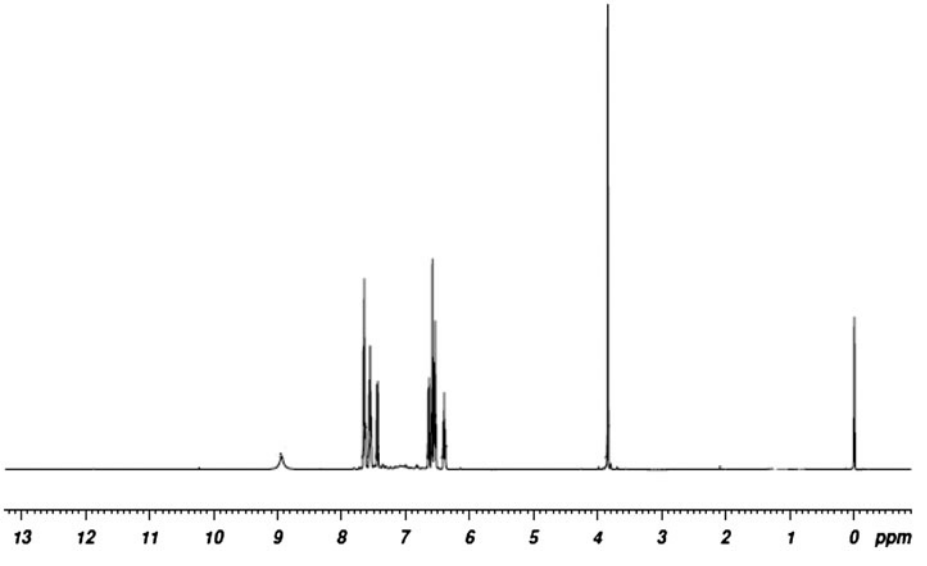

Figure 2. ^{1}H NMR spectrum of Zn(II) complex (**1e**).

3.3. *^{1}H NMR study*

^{1}H NMR spectra of HL and **1e** were recorded in DMSO-d_6 using TMS as a reference. The absence of the signal for phenolic OH in the spectrum of **1e** confirms coordination of phenolic–O to Zn(II) (figure 2). Also, no peaks are found at 4.69–4.82 ppm in the complex, indicating the absence of coordinated water. The signal at 10.62 ppm is present in both the spectra of ligand and its Zn(II) complex, which is due to the presence of another phenolic–OH.

3.4. *FAB-mass spectral study*

FAB-mass of metal(II) complexes were recorded and the obtained molecular ion (*m/z*) peaks confirm the proposed formulas. A representative mass spectrum of **1c** is shown in figure 3. The complex exhibits (*m/z*) at 701 with [*M* + 2] pattern, which reinforces the data obtained by microanalysis.

3.5. *EPR spectra of copper complex (1d)*

X-band EPR spectra of Cu(II) complex (**1d**) were recorded in DMSO at ambient and low (300 and 77 K) temperatures. At 300 K, EPR spectrum exhibits well-resolved hyperfine structures due to magnetic coupling between the unpaired electron with effective ^{63,65}Copper nuclei (I = 3/2). Frozen (77 K) EPR spectrum shows anisotropic pattern, i.e. four well-resolved peaks which may be assigned to monomeric Cu(II) complexes [38, 39]. Axial symmetry with g-tensor value follows the order, $g_{\|}$ (2.23) > $g_{\perp}$ (2.02) > g_e (2.0023), indicating that the unpaired electron is localized in the $d_{x^2-y^2}$ orbital [39, 40] with $3d^9$ configuration and the observed g values are less than 2.3, indicating covalent Cu–L bond [41].

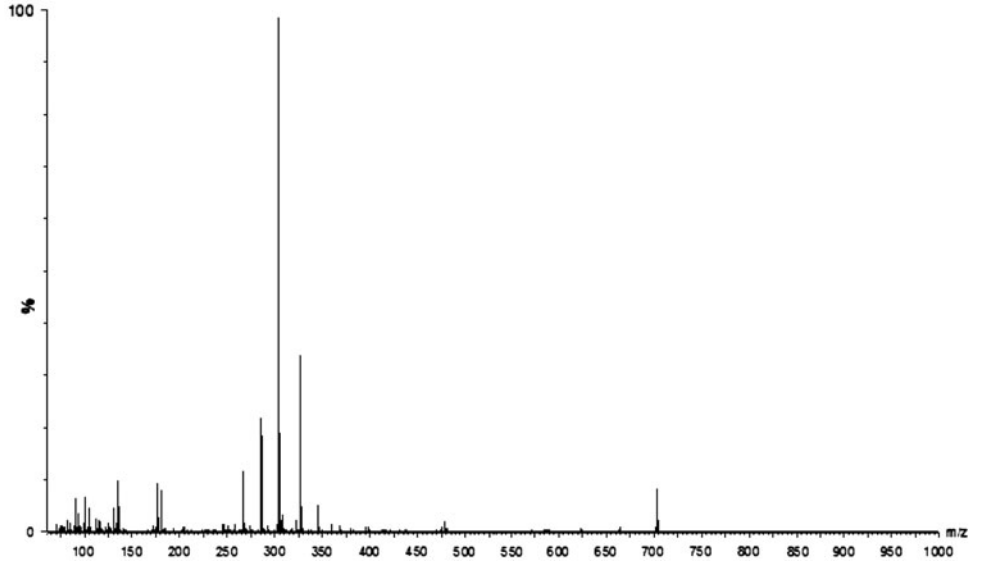

Figure 3. FAB-mass spectrum of Ni(II) complex (**1c**).

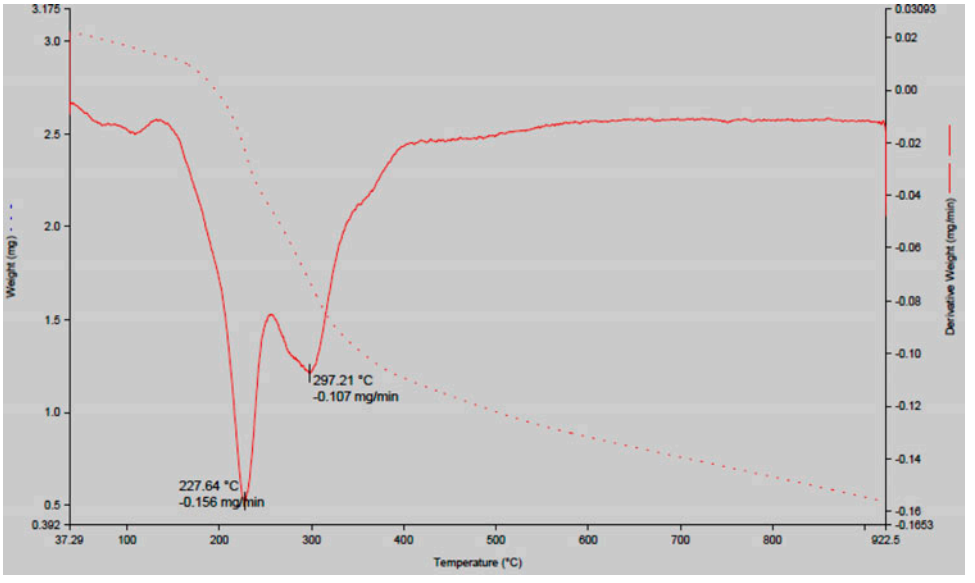

Figure 4. Thermogravimetric pictogram of **1d**.

Calculated g_{avg} value (2.09) deviates from the g_e value due to the covalent property. The absence of any half-field signal at 1600 G corresponding to Δ Ms = ±2 transitions rules out any magnetic exchange, i.e. Cu–Cu interactions in the complexes. This is further supported from the G value [42], if the value is less than four, the exchange interaction is considerable. In the present case, G of 3.64 implies that the exchange interaction is considerable and may be due to parallel or slightly misaligned environment of local tetragonal axes. Bonding parameters (α^2 = 0.63 and β^2 = 0.91) clearly indicate that the σ-bonding is more covalent than in-plane π-bonding [43]. Also the observed $A_{\|}$ (126 × 10^{-4} cm) value is comparable to reported tetrahedral Cu(II) complexes [44, 45]. Geometry of **1d** was further confirmed by the empirical ratio value ($g_{\|}/A_{\|}$ = 172 cm) and this value is similar to reported values [44] with tetrahedral environments around the Cu(II).

3.6. *Thermal analyses*

Thermogravimetric (TGA/DTA) analyses have been studied from ambient to 900 °C for **1c** and **1d** under air. A thermogram of **1d** is shown in figure 4. Thermal decomposition of **1c** occurs in three steps whereas **1d** occurs in only two steps. The first loss in weight occurs from 85 to 185 °C. This behavior is typical of the presence of coordinated water [46]. There is no loss in weight up to 200 °C, revealing the absence of any crystal and coordinated water in **1d**. In **1c** and **1d**, loss in weight at 365–410 °C of 38.7–40.1% corresponds to evaporation of organic moiety. In all cases, decomposition of the ligand continues leading to formation of air stable metal oxide as the end product at 600–810 °C. The results are in accord with the composition of the metal complexes. Kinetic order of the decomposition of Schiff base metal(II) complexes is also calculated by the modified Horowitz and Metzger equation as: $[C_s = (W_s - W_f)/(W_o - W_f)]$. The observed C_s value (0.64–0.70) indicates that the decomposition follows first-order kinetics.

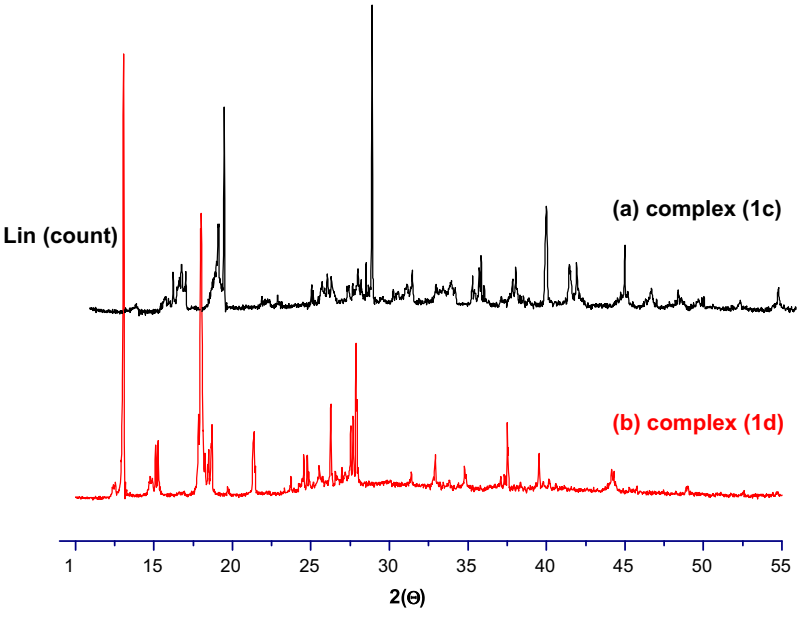

Figure 5. XRD powder pattern of (a) **1c** and (b) **1d**.

3.7. *Powder XRD and SEM analysis*

Powder XRD studies and SEM analysis are useful to determine the structure, particle size, and morphology of the synthesized complexes. The powder X-ray diffractograms of **1c** and **1d** are given in figure 5. The observed diffractograms show a uniform phase with no impurity. Also the XRD pattern shows slightly crystalline nature of the metal complexes. Crystallite sizes of the complexes are estimated from the main XRD peak using Scherrer's equation [47, 48] as: $D = 0.9\lambda/\beta\cos\theta$. Observed average crystallite sizes of **1c** and **1d** were 46 and 53 nm, respectively.

Morphology and particle size of the Schiff base metal(II) complexes have been illustrated from the SEM. Figure 6 depicts the SEM photographs of **1c** and **1d**. The morphology of

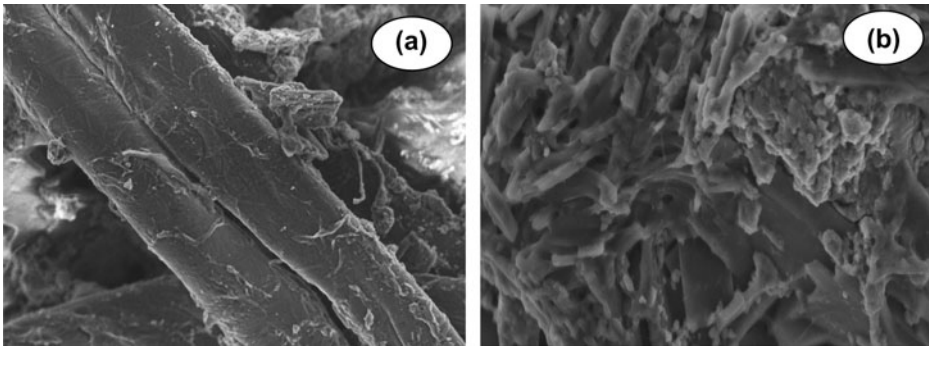

Figure 6. SEM photographs of (a) Ni(II) and (b) Cu(II) complexes.

free Schiff base shows macroscopic phase separation with the particle size of 20–30 μm. This phase separation is reduced after the formation of Schiff base metal(II) complexes and also reduced the particle size of 10–20 μm. This change in the surface morphology indicates the formation of Schiff base metal(II) complexes. From SEM pictographs, all the complexes have uniform matrix with smooth interface having regular shape of homogeneous phase material. A wrecked rod-like shape is observed in **1c** with the particle size of 15 μm. Particle size of **1d** is obtained as 10 μm with a mixture of broken pieces having ice-like shape, indicating we are dealing with homogeneous material.

3.8. *Biological activity*

In vitro biological activities of HL and **1a**–**1e** were tested against bacterial and fungal strains by well diffusion method using agar as nutrient. Commercially available standard drugs Ampicillin (antibacterial control) and Nystatin (antifungal control) are used as controls. Measurement of zone of inhibition against the growth of bacteria and fungi for the ligand and its complexes is given in table 3 and a representative graph is shown in figure 7. All the complexes show biological activities at higher concentration (50 μg) against microorganisms. Higher inhibition zones of the ligand and its complexes can be explained on the basis of Overtone's concept and Tweedy's chelation theory [49]. All the complexes show more antibacterial and less antifungal activities. Biological activities of the metal complexes increase as the stability of the complexes increased. The activity of HL and its metal complexes follows the order as:

$$\text{Control} > \mathbf{1d} > \mathbf{1c} > \mathbf{1b} \approx \mathbf{1e} > \mathbf{1a} > \text{HL}$$

3.9. *Antioxidant activity*

In vitro antioxidant activities of HL and its metal(II) complexes were tested by DPPH free radical scavenging method, and ascorbic acid was used as the reference or positive control. All analyses were done in three replicates and their representative graph is shown in figure 8. Reduction capability of free radical (DPPH) is determined by the decrease in its absorbance at 517 nm (blank), which can be induced by an antioxidant. From the results, it is seen that the Schiff base metal(II) complexes have higher activities than HL [50].

3.10. *DNA binding studies*

3.10.1. Electronic absorption study. Electronic absorption spectral technique was used to investigate the interaction of **1a**–**1e** with CT DNA. Electronic spectrum of copper complex (**1d**) in the absence and presence of CT DNA is shown in figure 9. Complex **1d** shows three bands at 245, 291, and 340 nm. During addition of CT DNA (varying the CT DNA concentration only), absorption intensity decreases (hypochromism) and wavelength increases slightly (bathochromism). Generally, hypochromism and bathochromism indicate that the metal complex binds with CT DNA through an intercalative mode and involves a strong interaction of aromatic chromophore of the complex with the base pairs of DNA [51]. The intrinsic binding constant and change in free energy values of **1a**–**1e** were

Table 3. Antimicrobial activity of HL and **1a**–**1e** by well-diffusion agar method.

	Zone of inhibition (in mm)																				
	E. coli			*S. saphyphiticus*			*S. aureus*			*P. aeruginosa*			*A. niger*			*E. species*			*C. albicans*		
Complexes	24 h	48 h	72 h	24 h	48 h	72 h	24 h	48 h	72 h	24 h	48 h	72 h	24 h	48 h	72 h	24 h	48 h	72 h	24 h	48 h	72 h
Control	13	14	15	15	16	17	16	17	18	15	16	17	16	17	18	19	21	22	18	20	21
HL	6	6	7	8	8	9	9	9	10	–	–	–	8	10	11	14	14	15	–	–	–
1a	8	9	10	–	–	–	11	12	13	10	11	12	10	12	12	13	14	14	15	16	16
1b	9	10	11	11	12	13	–	–	–	11	12	13	–	–	–	11	12	14	–	–	–
1c	10	10	12	12	12	14	13	13	15	–	–	–	12	13	14	–	–	–	16	16	17
1d	11	12	14	13	14	16	14	15	17	13	14	16	–	–	–	15	16	18	17	18	20
1e	10	10	11	12	12	13	13	13	14	12	12	13	–	–	–	–	–	–	–	–	–

Note: [–] = Less active, error limit: ±2%.

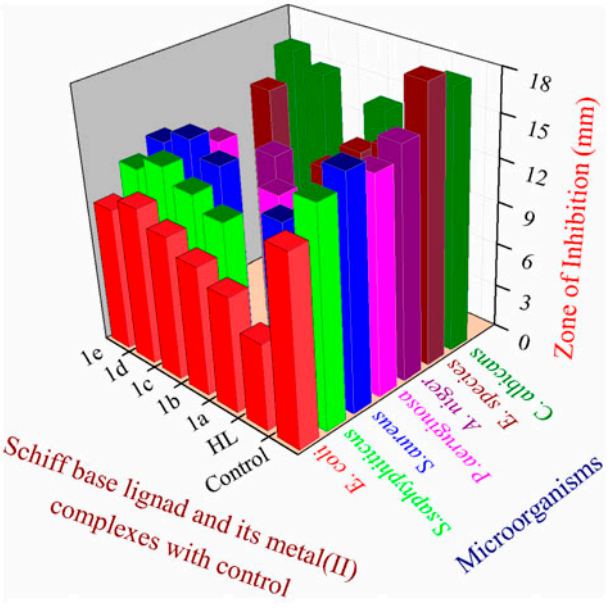

Figure 7. Biological activities of HL and **1a**–**1e** with different micro-organisms at 24 h.

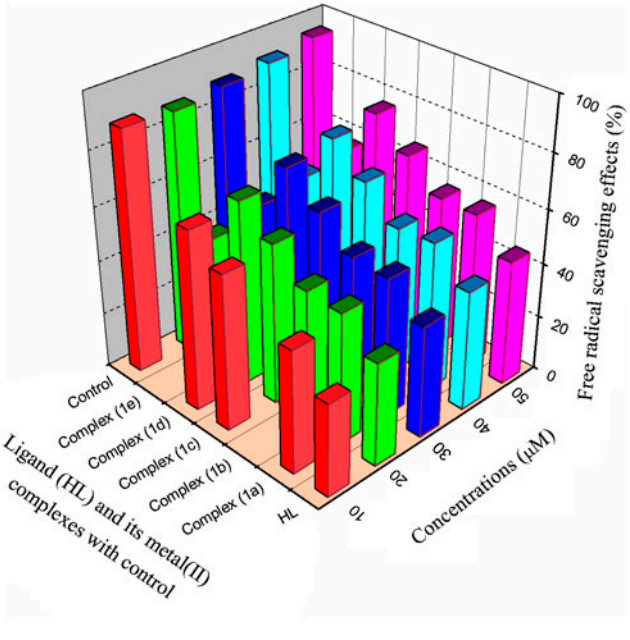

Figure 8. *In vitro* antioxidant activities of HL and its metal(II) complexes by DPPH free radical scavenging assay method at 10–50 μM.

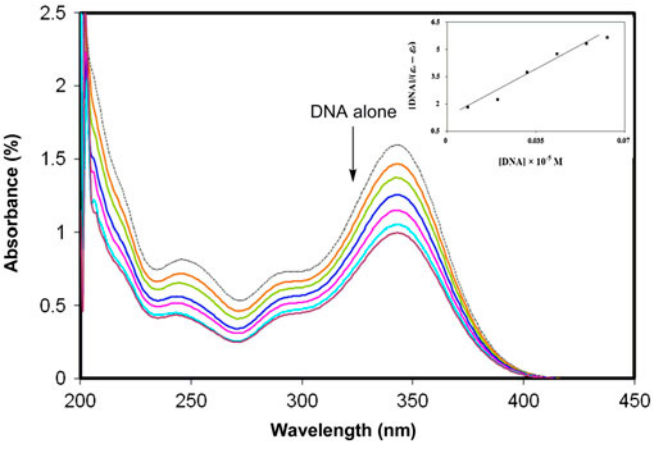

Figure 9. Electronic absorption spectrum of **1d** in the absence (—) and presence (—) of increasing amount of CT DNA. Inset is a typical plot of [DNA]/($\varepsilon_a - \varepsilon_f$) *vs.* [DNA] for the determination of equilibrium-binding constants (K_b).

Table 4. Intrinsic binding constant (K_b) values of **1a**–**1e**.

Complexes	λ_{max} (nm)		$\Delta\lambda$ (nm)	% H	$K_b \times 10^2$ (M^{-1})	ΔG (KJ M^{-1})
	Free	Bound				
1a	343.0	344.2	1.2	8	5.42	−16.23
1b	342.5	343.8	1.3	10	6.64	−16.75
1c	343.0	344.2	1.2	8	5.55	−16.29
1d	343.0	344.8	1.8	15	7.78	−17.16
1e	342.8	343.8	1.0	9	5.89	−16.44

determined (table 4) from the plot of [DNA] *versus* [DNA]/($\varepsilon_a - \varepsilon_f$). The data indicate that these complexes are moderate intercalators when compared to the available literature values [52–54].

3.10.2. Fluorescence study. Fluorescence spectra are also used to study the interaction between the metal(II) complexes with DNA by measuring the emission intensity of EB bound to DNA. EB is weakly fluorescent, but can emit intense fluorescence in the presence of DNA due to its intercalative binding to DNA. However, this enhanced fluorescence can be quenched or partially quenched by addition of a second molecule that can replace the bound EB or break the secondary structure of DNA [55]. So, EB can be used as a probe for determination of DNA structure. In this study, the emission spectrum of EB bound to DNA in the absence and presence of **1d** was recorded. The results show that the fluorescence intensity of DNA–EB decreases remarkably with the addition of **1d** indicating that the complex binds to DNA by intercalation or partial intercalation replacing EB from the DNA structure.

3.11. *Oxidative cleavage study*

Cleavage efficiency of the metal(II) complexes with *pUC* 19 DNA was studied by gel electrophoresis in the presence of an oxidant (H_2O_2). A representative cleavage pictograph of **1a–1e** is shown in figure 10. Control experiment using *pUC* 19 DNA alone (Lane 1) does

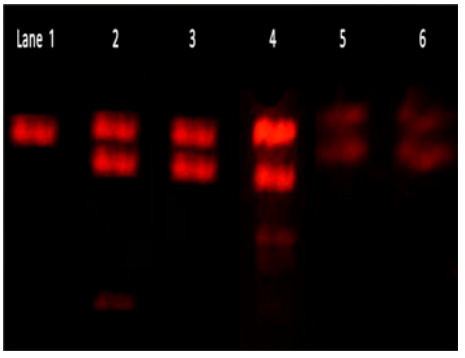

Lane 1: DNA alone
Lane 2: Complex **1a** + DNA + H_2O_2
Lane 3: Complex **1b** + DNA + H_2O_2
Lane 4: Complex **1d** + DNA + H_2O_2
Lane 5: Complex **1c** + DNA + H_2O_2
Lane 6: Complex **1e** + DNA + H_2O_2

Figure 10. Changes in the agarose gel electrophoresis pattern of *pUC* 19 DNA induced by **1a**–**1e** with H_2O_2.

not show any significant cleavage even on longer exposure time. In general, the oxidative cleavage is proposed to account for *pUC* 19 DNA cleavage caused by M(II) ions reacting with H_2O_2 to produce diffusible hydroxyl radicals or molecular oxygen or peroxy derivative. Cleavage is inhibited by free radical via the abstraction of a hydrogen from sugar units (at C_4' position) and predicts the release of specific residues arising from transformed sugars, depending on the position from which the hydrogen is removed and finally cleaves *pUC* 19 DNA [56]. From the pictograph**,** the results show that **1a**, **1b**, and **1d** have the ability to cleave the *pUC* 19 DNA in the presence of oxidant.

4. Conclusion

HL coordinates to metal(II) ions through N and O, and the formed metal(II) complexes have 1 : 2 (metal : Schiff base) stoichiometry. They are characterized using various physicchemical and spectral techniques. Electronic absorption studies coupled with magnetic moment values reveal that **1a**–**1c** adopt octahedral geometry with two water molecules in the coordination sphere while the Cu(II) and Zn(II) complexes (**1d** and **1e**) adopt tetrahedral geometry without coordinated water. *In vitro* antimicrobial activities show that the complexes are more active than HL. The complexes bind with DNA through an intercalative mode. Oxidative DNA cleavage reveals that Mn(II), Co(II), and Cu(II) complexes have significant ability to cleave the *pUC* 19 DNA in the presence of oxidant.

Acknowledgements

We express our sincere thanks to the College Managing Board, Principal, and Head of the Department of Chemistry, Devanga Arts College, Aruppukottai and VHNSN College, Virudhunagar for providing research facilities. They express their gratitude to SAIF, IIT Madras, IIT Bombay, and Punjab University for recording NMR, EPR, and FAB-mass spectra, respectively, and STIC, Cochin for TGA/DTA and SEM studies.

References

[1] B. Selvakumar, V. Rajendiran, P.U. Uma Maheswari, H. Stoeckli-Evans, M. Palaniandavar. *J. Inorg. Biochem.*, **100**, 316 (2006).
[2] M. Yodoshi, M. Odoko, N. Okabe. *Chem. Pharm. Bull.*, **55**, 853 (2007).
[3] A.A. Khandar, K. Nejati. *Polyhedron*, **19**, 607 (2000).
[4] L. Nathan, J.E. Koehne, J.M. Gilmore, K.A. Hannibal, W.E. Dewhirst, T.D. Mai. *Polyhedron*, **22**, 887 (2003).
[5] S.N. Pandeya, D. Sriram, G. Nath, E. De Clercq. *Il Farmaco*, **54**, 624 (1999).
[6] B.N. Berad, M.R.S. Deshmukh, C.S. Bhaskar. *Asian J. Chem.*, **14**, 1241 (2002).
[7] Z.M. Nofal, M.I. El-Zahar, S.S. Abd El-Karim. *Molecules*, **5**, 99 (2000).
[8] S. Samadhiya, A. Halve. *Orient J. Chem.*, **17**, 119 (2001).
[9] M.R. Boyd, R.W. Fuller, C.K. Westergaard, J.W. Collines, J.H.R. Cardilina. *Nat. Prod.*, **62**, 67 (1999).
[10] N. Raman, S. Sobha, A. Thamaraichelvan. *Spectrochim. Acta, Part A*, **78**, 888 (2011).
[11] N. Raman, R. Jeyamurugan, R. Senthilkumar, B. Rajkapoor, S.G. Franzblau. *Eur. J. Med. Chem.*, **45**, 5438 (2010).
[12] P. Subbaraj, A. Ramu, N. Raman, J. Dharmaraja. *Spectrochim. Acta, Part A*, **117**, 65 (2014).
[13] N. Raman, K. Pothiraj, T. Baskaran. *J. Coord. Chem.*, **64**, 4286 (2011).
[14] S.M. Abdallah. *Arab. J. Chem.*, **5**, 251 (2012).
[15] G. Ceyhan, C. Çelik, S. Uruş, İ. Demirtaş, M. Elmastaş, M. Tümer. *Spectrochim. Acta, Part A*, **81**, 184 (2011).
[16] D. Arish, M. Sivasankaran Nair. *J. Coord. Chem.*, **63**, 1619 (2010).
[17] M. Roy, A.K. Patra, A. Mukherjee, M. Nethaji, A.R. Chakravarty. *Ind. J. Chem.*, **46A**, 227 (2007).
[18] J. Reedijk. *J. Inorg. Biochem.*, **86**, 1411 (2001).
[19] S. Sathiyaraj, R.J. Butcher, C. Jeyabalakrishnan. *J. Mol. Struct.*, **1030**, 95 (2013).
[20] D.D. Perrin, W.L.F. Armarego, D.R. Perrin. *Purification of Laboratory Chemicals*, Pergamon Press, Oxford (1980).
[21] A. Earnshaw. *Introduction to Magneto Chemistry*, Academic Press, New York (1968).
[22] M.J. Pelczar, E.C.S. Chan, N.R. Krieg. *Microbiology*, 5th Edn, Tata Mc-Graw Hill, New Delhi (1998).
[23] M.S. Blois. *Nature*, **181**, 1199 (1958).
[24] A. Hussain, S. Saha, R. Majumdar, R.R. Dighe, A.R. Chakravarty. *Ind. J. Chem.*, **50A**, 519 (2011).
[25] D. Crespy, K. Landfester, U.S. Schubert, A. Schiller. *Chem. Commun.*, **46**, 6651 (2010).
[26] N.J. Farrer, L. Salassa, P.J. Sadler. *Dalton Trans.*, 10690 (2009).
[27] J. Marmur. *J. Mol. Biol.*, **3**, 208 (1961).
[28] A. Wolfe, G.H. Shimer Jr., T. Meehan. *Biochemistry*, **26**, 6392 (1987).
[29] S. Zhang, J. Zhou. *J. Coord. Chem.*, **61**, 2488 (2008).
[30] W.J. Geary. *Coord. Chem. Rev.*, **7**, 81 (1971).
[31] L.J. Bellamy. *The Infrared Spectra of Complex Molecules*, 2nd Edn, Chapman & Hall, Methuen, MA (1958).
[32] K. Nakamoto. *Infrared Spectra of Inorganic and Coordination Compounds, Part B*, 5th Edn, Wiley Interscience, New York (1997).
[33] J.R. Ferraro. *Low-frequency Vibrations of Inorganic and Coordination Compounds*, Plenum Press, New York (1971).
[34] T.M. Dunn. *The Visible and Ultraviolet Spectra of Complex Compounds in Modern Coordination Chemistry*, Wiley Interscience, New York (1960).
[35] A.B.P. Lever. *Inorganic Electronic Spectroscopy*, Elsevier, New York (1984).
[36] B.N. Figgs. *Introduction to Ligand Field*, Wiley, New York (1966).
[37] C.J. Ballhausen. *An Introduction to Ligand Field Theory*, McGraw Hill, New York (1962).
[38] R.S. Drago, M.J. Desmond, B.B. Corden, K.A. Miller. *J. Am. Chem. Soc.*, **105**, 2287 (1983).
[39] B.R. McGarvey. In *Transition Metal Chemistry*, R.L. Carlin (Ed.), Marcel Dekker, New York (1966).
[40] A. Abragam, B. Bleaney. *Electron Paramagnetic Resonance of Transition Ions*, Clarendon Press, Oxford (1970).
[41] S. Balasubramanian, C.N. Krishnan. *Polyhedron*, **5**, 669 (1986).
[42] B.J. Hathaway, A.A.G. Tomlinson. *Coord. Chem. Rev.*, **5**, 1 (1970).
[43] A.M.F. Benial, V. Ramakrishnan, R. Murugesan. *Spectrochim. Acta, Part A*, **56**, 2775 (2000).
[44] A.W. Addison, In *Coordination Chemistry: Bio Chemical and Inorganic Perspectives*, K.D. Karlin, J. Zubieta (Eds), Academic Press, New York (1983).
[45] W.A. Alves, R.H. Santos, A. Paduan-Filho, C.C. Becerra, A.C. Borin, A.M.D. Ferreira. *Inorg. Chim. Acta*, **357**, 2269 (2004).
[46] C. Duval. *Inorganic Thermogravimetric Analysis*, 2nd Edn, Elsevier, Amsterdam (1963).
[47] B.D. Cullity. *Elements of X-ray Diffraction*, 2nd Edn, Addison-Wesley, Reading, MA (1978).
[48] A. Guinier. *X-ray Diffraction in Crystals, Imperfect Crystals, and Amorphous Bodies*, W.H. Freeman & Company, San Francisco, CA (1963).
[49] B.G. Tweedy. *Phytopathology*, **55**, 910 (1964).
[50] D. Meyerstein. *J. Coord. Chem.*, **66**, 2076 (2013).

[51] S.A. Tysoe, R.J. Morgan, A.D. Baker, T.C. Strekas. *J. Phys. Chem.*, **97**, 1707 (1993).
[52] X. Fan, J. Dong, R. Min, Y. Chen, X. Yi, J. Zhou, S. Zhang. *J. Coord. Chem.*, **66**, 4268 (2013).
[53] D.D. Li, Z.W. Tao. *J. Coord. Chem.*, **66**, 4237 (2013).
[54] Z.B. Ou, Y.H. Lu, Y.M. Lu, S. Chen, Y.H. Xiong, X.H. Zhou, Z.W. Mao, X.Y. Le. *J. Coord. Chem.*, **66**, 2152 (2013).
[55] Y.F. Song, P. Yang. *Polyhedron*, **20**, 501 (2001).
[56] G. Pratviel, M. Pitié, J. Bernadou, B. Meunier. *Angew. Chem. Int. Ed. Engl.*, **30**, 702 (1991).